




Preparation of NaNbO_3 nanoplates and their application in the synthesis of arylidene indan-1,3-diones, functionalized C-3 isobenzofuranones and Meldrum's acid derivatives

Silma Francielle da Silva¹, Felipe Anchieta e Silva², Ana Paula Martins de Souza¹,
Thenner Silva Rodrigues^{2,*}, and Róbson Ricardo Teixeira^{1,*} 

¹Department of Chemistry, Universidade Federal de Viçosa, Av. P. H. Rolfs, S/N, Viçosa, MG 36570-900, Brazil

²Nanotechnology Engineering Program, Alberto Luiz Coimbra Institute for Graduate Studies and Research in Engineering, COPPE, Federal University of Rio de Janeiro, Av. Horácio Macedo, 2030, Rio de Janeiro, RJ 21941-972, Brazil

Received: 26 July 2021

Accepted: 8 November 2021

Published online:

3 January 2022

© The Author(s), under exclusive licence to Springer Science+Business Media, LLC, part of Springer Nature 2021

ABSTRACT

The present investigation describes the preparation of a sodium niobate nanostructured material and the application of it as catalyst in condensation reactions. Well-defined NaNbO_3 nanoplates were obtained via a basic hydrothermal process using $\text{Nb}_2\text{O}_5 \cdot n\text{H}_2\text{O}$ as starting material. The NaNbO_3 nanostructured catalyst was characterized by scanning electron microscopy (SEM) and X-ray diffractometry (XRD), N_2 adsorption/desorption isotherms, and hydrogen temperature-programmed reduction (H_2 -TPR) analysis. The performance of NaNbO_3 as a catalyst was evaluated in condensation reactions for the preparation of 2-arylidene indan-1,3-diones, C-3 functionalized isobenzofuran-1(3H)-ones, Meldrum's acid derivatives, and a coumarin. The products obtained in these reactions present several important bioactivities and are useful building blocks in organic synthesis. The condensation reactions were run under microwave irradiation and without the use of solvents. The compounds prepared in the condensation reactions were purified by recrystallization and obtained with satisfactory yields and short reaction times. The catalyst can be recycled in the condensation processes.

Handling Editor: Andrea de Camargo.

Silma Francielle da Silva and Felipe Anchieta e Silva have contributed equally.

Address correspondence to E-mail: thenner@pent.coppe.ufrj.br; robsonr.teixeira@ufv.br

Introduction

According to the Brazilian Metallurgy and Mining Company (CBMM), Brazil holds 85% of the world's niobium reserves (730000 tons), followed by Canada with 1600000 tons. The niobium mine production is estimated to be 69100 tons annually worldwide, being 60700 tons produced in Brazil [1]. The great biocompatibility, lower toxicity of niobium, and high strength promote the development of new artificial implants in orthopedic and dental materials [2–4]. In terms of compound compositions, four different charge states are described for niobium: 0 (Nb), 2 + (NbO), 4 + (NbO₂), and 5 + (Nb₂O₅). Because of its electronic structure and coordination number, the most stable oxidation state is 5 + , as in the niobium pentoxide (Nb₂O₅) which is one of the most attractive niobium compounds [5]. Due to its special variety of electrotonic structure, niobium-based nanomaterials have proven to be an important component in catalytic applications, such as oxidation of cyclohexene, oxidation of glycerol, and in the production of acrylic acid [6, 7].

In this context, Nb₂O₅ nanomaterials are extensively employed and their synthesis can be provided by Sol-Gel, polymeric precursor, co-precipitation, and hydrothermal methods [8–11]. The polymorphism of Nb₂O₅ can be controlled by changing the method for its synthesis and variation parameters that include type of Nb precursor, solvent, precipitating agent, pressure, and principally, temperature, in which until 900 °C T-Nb₂O₅ is mostly observed, between 900 and 1100 °C, the M-Nb₂O₅ phase is preferentially formed, and above 1100 °C, the H-Nb₂O₅ is achieved [12, 13]. However, some other compounds can be obtained from the Nb₂O₅, which can act as starting material to produce other oxides and compounds, including niobium halides, niobic acid, and niobates that are strongly effective for catalytic applications, due to their special performances and stabilities [14–16]. In this sense, sodium niobate (NaNbO₃) has attracted special attention and has been synthesized by different methods, such as Sol-Gel, solid-state, microemulsion-mediated, solvothermal, and hydrothermal processes. Different Nb-sources are employed in this way, for example, Nb powder, Nb(OC₂H₅)₅, and Nb₂O₅. Among the above-mentioned protocols, hydrothermal method is considered one of the best options for the synthesis of

NaNbO₃. In this case, H₂O, Nb₂O₅, and NaOH are employed as reactants at relatively low temperatures (~ 100 – ~ 200 °C) [17–21]. In this type of method, temperature and NaOH concentration are pointed as the key elements for the preparation of NaNbO₃ nanoparticles displaying well-defined and controlled morphologies and sizes. By the variation on these parameters, it is possible to synthesize NaNbO₃ nanorods, nanosheets, and nanocubes, for example [22, 23].

It is well-established that NaNbO₃ exhibits orthorhombic distorted perovskites structure, anti-ferroelectric properties at room temperature, and photochemical activity, which justify its utilizations in a variety of technological applications, in which these properties are demanded [18, 24]. However, NaNbO₃ nanoparticles have also been applied in heterogeneous catalysis as a catalyst by itself, such as NaNbO₃ nanowires [25], and also as support for the incorporation of active sites leading to the formation of nanocomposites, such as Ru/NaNbO₃ [26] and Ag/NaNbO₃. [24] Within this context, we present herein the preparation of NaNbO₃ nanoplates using a commercial Nb₂O₅ as starting material via a hydrothermal process. Considering our research interest in the synthesis, structural features, and biological activities of indandiones and isobenzofuranones [27–41], the catalytic performance of NaNbO₃ nanoplates was evaluated in condensation reactions for the preparation of 2-arylidene indan-1,3-diones and functionalized C-3 isobenzofuran-1(3H)-ones. Besides, the efficiency of NaNbO₃ nanostructure catalyst was also evaluated in the synthesis of Meldrum's acid derivatives, and the results are discussed.

Experimental section

Materials and instrumentation

Analytical grade indan-1,3-dione (C₉H₆O₂, 97%, Sigma-Aldrich), hydrated niobium acid (Nb₂O₅·nH₂O, 81%, CBMM), 2-carboxy benzaldehyde (phthalaldehydic acid) (C₈H₆O₃, 97%, Sigma-Aldrich), Meldrum's acid (C₆H₈O₄, 98%, Sigma-Aldrich), 4-chloro benzaldehyde (ClC₆H₄CHO, 97%, Sigma-Aldrich), 4-bromo benzaldehyde (BrC₆H₄CHO, 99%, Sigma-Aldrich), 4-nitro benzaldehyde (O₂NC₆H₄CHO, 98%, Sigma-Aldrich), 4-fluoro benzaldehyde

(FC₆H₄CHO, 98%, Sigma-Aldrich), 4-methoxy benzaldehyde (CH₃OC₆H₄CHO, 98%, Sigma-Aldrich), benzaldehyde (C₆H₄CHO, ≥ 99%, Sigma-Aldrich), 4-hydroxy benzaldehyde (HOC₆H₄CHO, 98%, Sigma-Aldrich), 3,4,5-trimethoxy benzaldehyde (CH₃O)₃C₆H₄CHO, 98%, Sigma-Aldrich), 2-hydroxy benzaldehyde (HOC₆H₄CHO, 98%, Sigma-Aldrich), 3-hydroxy benzaldehyde (HOC₆H₄CHO, ≥ 99%, Sigma-Aldrich), 4-hydroxy-3-methoxy benzaldehyde (HOC₆H₃(OCH₃)CHO, 97%, Sigma-Aldrich), 1,3-cyclohexanedione (C₆H₈O₂, 97%, Sigma-Aldrich), 5-methyl-1,3-cyclohexanedione (C₇H₁₀O₂, 98%, Sigma-Aldrich), 5,5-dimethyl-1,3-cyclohexanedione (dimedone) (C₈H₁₂O₂, 95%, Sigma-Aldrich), and 1,3-cyclopentanedione (C₅H₆O₂, 97%, Sigma-Aldrich) were used as received. The solvents (ethanol, C₂H₆O, 99%; hexane, C₆H₁₄—a mixture of isomers; ethyl acetate, C₄H₈O₂, 99.5%; dichloromethane, CH₂Cl₂, 99.5%; acetone, C₃H₆O, 99.5%) were purchased from Vetec, Brazil.

The scanning electron microscopy (SEM) images were obtained using a JEOL field emission gun electron microscope JSM6330F operated at 5 kV. Energy dispersive spectroscopy (EDS) analyses and scanning transmission electron microscopy (STEM) images were obtained using a Tescan VEGA 3 LMU scanning electron microscope operated at 20 kV. High-resolution transmission electron microscopy (HRTEM) images were obtained using an FEI TECNAI T20 scanning electron microscope operated at 200 kV. The samples were prepared by drop-casting an aqueous suspension containing the structure over a copper grid or over a silicon wafer, followed by drying under ambient conditions. X-ray diffractometry (XRD) measurements were performed on a Rigaku model Miniflex equipment using a CuK α radiation (30 kV, 15 mA, $\lambda = 0.15418$ nm). The diffraction patterns were measured between 10° and 90° 2 θ with a step size of 0.02° 2 θ . The textural properties of the materials were determined from N₂ adsorption/desorption isotherms, Micrometrics ASAP 2020 surface area analyzer and porosity analyzer equipment. The samples were pretreated at 300 °C for 2 h, and then degassed under vacuum. The values of the specific surface areas were determined from the Brunauer-Emmett-Teller (BET) equation. The total pore volume was determined by the adsorption isotherms using the model proposed by Barrett-Joyner-Halenda (BJH). Hydrogen temperature-programmed reduction (H₂-TPR) analyses were

performed using a Micrometrics Chemisorb 2705 equipment. In the analyses, 50 mg of material was used at a temperature ramp of 25 to 1100 °C at 10 °C min⁻¹ and a flow of 30 mL min⁻¹ of 5% H₂/N₂. Samples were pretreated at 200 °C for 2 h under He flow. The surface basicity was determined by temperature-programmed desorption of CO₂ (CO₂-TPD) in a multipurpose unit with a Pfeiffer Vacuum Prisma detector mass spectrometer. Typically, 0.1 g of solid material was dried with He flow at 200 °C for 0.5 h and then cooled down to room temperature. The solid was reduced with H₂ flow at 500 °C for 1 h, then kept with He flow for 1 h and cooled down to room temperature. CO₂ was adsorbed with a CO₂ flow at room temperature for 0.5 h. The catalysts were cleaned with He flow for 1 h. Finally, the temperature ramp of 25 to 800 °C at 20 °C min⁻¹ was utilized. The surface acidity was determined by temperature-programmed desorption of NH₃ (NH₃-TPD) in a multipurpose unit with a Pfeiffer Vacuum Prisma detector mass spectrometer. Typically, 0.1 g of solid material was dried with He flow at 200 °C for 0.5 h and then cooled down to room temperature. The solid material was reduced with H₂ flow at 500 °C for 1 h, then kept with He flow for 1 h and cooled down to room temperature. NH₃ was adsorbed with a 4% NH₃/He flow at room temperature for 0.5 h. The solid material was treated with He flow for 1 h. Finally, the temperature ramp of 25 to 800 °C at 20 °C min⁻¹ was employed.

¹H-NMR (300 MHz) and ¹³C-NMR (75 MHz) spectra were recorded on a Varian Mercury 300 instrument. ¹H-NMR (400 MHz) and ¹³C-NMR (100 MHz) spectra were acquired on Bruker AVANCE DRX 400 spectrometer. ¹H-NMR (200 MHz) and ¹³C-NMR (50 MHz) spectra were acquired on Bruker AVANCE DPX 200 spectrometer. For the NMR spectrum acquisition, CDCl₃, MeOH-*d*₄, and DMSO-*d*₆ were used as solvents. NMR data are presented as follows: chemical shift (δ) in ppm, number of hydrogens, multiplicity, *J* values in Hertz (Hz). Multiplicities are shown as the following abbreviations: s (singlet), d (doublet), dd (doublet of doublets) dd_{ap} (apparent doublet of doublets), t (triplet), brs (broad singlet), t_{ap} (apparent triplet), t (triplet), and m (multiplet). IR spectra were obtained using Varian 660-IR equipped with GladiATR scanning from 4000 to 500 cm⁻¹. Analytical thin-layer chromatography analysis was conducted on aluminum backed pre-coated silica gel plates using

different solvent systems and was visualized using UV light. Reactions heated via microwave irradiation were conducted in a CEM Discover microwave reactor. Melting points were determined using MQAPF-301 melting point apparatus and were not corrected.

Synthesis of NaNbO_3 nanoplates

Niobium-based nanostructured catalyst was prepared using a procedure similar to that described by Dos Reis et al. [42] In a typical procedure, 2.00 g of commercial powdered $\text{Nb}_2\text{O}_5 \cdot n\text{H}_2\text{O}$ and 25 mL of 10 mol L^{-1} NaOH aqueous solution were added to a glass pressure vessel. After sealing the vessel, the mixture was heated at 150 °C under vigorous stirring for 72 h. After this period, the mixture was cooled down to room temperature and then washed with distilled water and vacuum filtered. To the obtained solid, 500 mL of aqueous HCl solution was added (pH = 2), and the resulting mixture was stirred for 24 h. After this period, the mixture was centrifuged, and the resulting solid was washed up three times with HCl (pH = 2) and three times with distilled water and oven-dried at 110 °C for 2 h.

Synthesis of indan-1,3-dione derivatives

Synthesis of 2-(4-chlorobenzylidene)-1H-indene-1,3(2H)-dione (1)

Indan-1,3-dione (150 mg, 1.00 mmol), 4-chloro benzaldehyde (144 mg, 1.00 mmol), and nanostructured NaNbO_3 (13.0 mg, 0.0800 mmol) were added to a sealed tube (10 mL). The reaction mixture was irradiated in the microwave reactor at 85 °C with a ramp time of 2 min, medium agitation, and using a closed system for 10 min. The reaction was monitored by thin-layer chromatography. After the completion of the reaction, dichloromethane was added to the mixture, followed by simple filtration. Compound 1 was obtained as a yellow solid in 70% yield (189 mg, 0.703 mmol) after recrystallization from dichloromethane–ethanol (1:1 v v⁻¹). The structure of 1 is supported by the following data.

Mp 175.9–177 °C (Lit.: 176.3–177.8 °C) [32]. IR (ATR) $\bar{\nu}$: 3091, 3064, 1725, 1918, 1887, 1725, 1684, 1576, 1071, 732, 427 cm^{-1} . ¹H-NMR (300 MHz, CDCl_3) δ : 7.47 (2H, d, J = 8.4 Hz), 7.81–7.83 (3H, m), 7.99–8.01 (2H, m), 8.41 (2H, d, J = 8.4 Hz). ¹³C-NMR (75 MHz,

CDCl_3) δ : 123.39, 123.41, 129.1, 129.4, 131.5, 135.3, 135.5, 139.5, 140.1, 142.5, 145.1, 188.9, 189.9.

Synthesis of indan-1,3-dione derivatives 2–11

A similar procedure to that described for the preparation of 1 was utilized to synthesize compounds 2–11. The structures of these compounds are supported by the following data.

2-(4-nitrobenzylidene)-1H-indene-1,3(2H)-dione

(2) Yellow solid, Mp 232.9–233.7 °C (Lit.: 233.1–233.6 °C) [32]. IR (ATR) $\bar{\nu}$: 3112, 3050, 1980, 1941, 1731, 1687, 1586, 1513, 1345, 855 cm^{-1} . ¹H-NMR (300 MHz, $\text{DMSO}-d_6$) δ : 7.93 (1H, s), 7.96–8.04 (4H, m), 8.33 (2H, d, J = 9.0 Hz), 8.58 (2H, d, J = 9.0 Hz). ¹³C-NMR (75 MHz, $\text{DMSO}-d_6$) δ : 123.79, 123.86, 132.9, 134.6, 136.7, 136.8, 138.9, 140.2, 142.0, 142.6, 149.3, 188.6, 189.2.

2-(4-bromobenzylidene)-1H-indene-1,3(2H)-dione

(3) Yellow solid, Mp 169.8–170.5 °C (Lit.: 169.7–170.3 °C) [32]. IR (ATR) $\bar{\nu}$: 3091, 3060, 1893, 1853, 1724, 1684, 1573, 1069, 827, 504 cm^{-1} . ¹H-NMR (300 MHz, CDCl_3) δ : 7.63 (2H, d, J = 8.7 Hz), 7.79 (1H, s), 7.81–7.83 (2H, m), 7.99–8.02 (2H, m), 8.32 (2H, d, J = 8.7 Hz). ¹³C-NMR (75 MHz, CDCl_3) δ : 123.41, 123.43, 128.3, 129.6, 131.9, 132.1, 135.4, 135.5, 140.1, 142.5, 145.2, 188.9, 189.9.

2-(4-methoxybenzylidene)-1H-indene-1,3(2H)-dione

(4) Yellow solid, Mp 155.5–156.6 °C. (Lit.: 155.3–156.8 °C) [32]. IR (ATR) $\bar{\nu}$: 3074, 2981, 2933, 1972, 1941, 1716, 1677, 1505, 1428, 1264, 1174, 1023, 837, 728 cm^{-1} . ¹H-NMR (300 MHz, CDCl_3) δ : 3.90 (3H, s), 7.00 (2H, d, J = 9.0 Hz), 7.76–7.80 (2H, m), 7.83 (1H, s), 7.93–8.00 (2H, m), 8.53 (2H, d, J = 9.0 Hz). ¹³C-NMR (75 MHz, CDCl_3) δ : 55.6, 114.4, 123.0, 126.4, 126.5, 134.8, 135.0, 137.1, 139.9, 142.3, 146.8, 164.0, 189.4, 190.7.

2-(4-hydroxybenzylidene)-1H-indene-1,3(2H)-dione

(5) Yellow solid, Mp 235.7–236.2 °C. (Lit.: 235.8–236.0 °C) [32]. IR (ATR) $\bar{\nu}$: 3363–3025 (broad band), 2954, 2885, 2024, 1976, 1716, 1656, 1553, 1512, 1206, 737 cm^{-1} . ¹H-NMR (300 MHz, $\text{DMSO}-d_6$) δ : 6.92 (2H, d, J = 8.7 Hz), 7.72 (1H, s), 7.86–7.92 (4H, m), 8.50 (2H, d, J = 8.7 Hz), 10.86 (1H, s). ¹³C-NMR (75 MHz, $\text{DMSO}-d_6$) δ : 116.4, 123.1, 123.2, 125.0, 125.6,

135.8, 135.9, 138.0, 139.6, 142.0, 146.7, 163.7, 189.4, 190.4.

2-(4-hydroxy-3-methoxybenzylidene)-1H-indene-1,3(2H)-dione (6) Yellow solid, Mp 215.5–216.2 °C (Lit.: 215.6–216.4 °C) [32]. IR (ATR) $\bar{\nu}$: 3550–3401 (broad band), 2981, 2942, 1911, 1870, 1707, 1655, 1562, 1299, 1137, 1019, 730 cm^{-1} . $^1\text{H-NMR}$ (300 MHz, $\text{DMSO-}d_6$) δ : 3.90 (3H, s), 6.93 (1H, *d*, *J* = 8.4 Hz), 7.72 (1H, *s*), 7.86–7.94 (5H, *m*), 8.68 (1H, *d*, *J* = 1.8 Hz). $^{13}\text{C-NMR}$ (75 MHz, $\text{DMSO-}d_6$) δ : 56.1, 116.1, 117.2, 123.1, 123.2, 125.4, 125.5, 132.1, 135.8, 135.9, 139.6, 142.1, 147.3, 147.8, 153.7, 189.6, 190.4.

2-benzylidene-1H-indene-1,3(2H)-dione (7) Yellow solid, Mp 150.6–151.1 °C. (Lit.: 150.6–150.8 °C) [32]. IR (ATR) $\bar{\nu}$: 3087, 3056, 2021, 1976, 1724, 1684, 1611, 1574, 1007, 827, 732, 583 cm^{-1} . $^1\text{H-NMR}$ (300 MHz, CDCl_3) δ : 7.48–7.58 (3H, *m*), 7.78–7.84 (2H, *m*), 7.89 (1H, *s*), 7.98–8.04 (2H, *m*), 8.44–8.46 (2H, *m*). $^{13}\text{C-NMR}$ (75 MHz, CDCl_3) δ : 123.3, 123.4, 128.8, 129.2, 133.1, 133.2, 134.1, 135.1, 135.3, 140.0, 142.5, 146.9, 188.9, 190.2.

2-(3,4,5-trimethoxybenzylidene)-1H-indene-1,3(2H)-dione (8) Orange solid, Mp 185.5–185.9 °C (Lit.: 185.4–185.6 °C) [32]. IR (ATR) $\bar{\nu}$: 3104, 2998, 2977, 2933, 1990, 1963, 1714, 1677, 1560, 1497, 1306, 1126, 731 cm^{-1} . $^1\text{H-NMR}$ (300 MHz, CDCl_3) δ : 3.98 (3H, *s*), 3.99 (6H, *s*), 7.78–7.81 (3H, *m*), 7.95 (2H, *s*), 7.97–7.99 (2H, *m*). $^{13}\text{C-NMR}$ (75 MHz, CDCl_3) δ : 56.3, 61.0, 112.0, 123.1, 123.2, 127.7, 128.4, 135.0, 135.2, 139.8, 142.4, 143.0, 147.3, 152.8, 189.4, 190.4.

2-(4-fluorobenzylidene)-1H-indene-1,3(2H)-dione (9) Yellow solid, Mp 179.8–181.2 °C (Lit.: 181.7 °C) [32]. IR (ATR) $\bar{\nu}$: 3070, 3039, 1986, 1967, 1727, 1686, 1617, 1198, 834, 731 cm^{-1} . $^1\text{H-NMR}$ (300 MHz, CDCl_3) δ : 7.18 (2H, *t*_{ap}, *J* = 8.7 Hz), 7.79 (1H, *s*), 7.80–7.83 (2H, *m*), 7.96–8.03 (2H, *m*), 8.52 (2H, *dd*_{ap}, *J*₁ = 8.7 Hz, *J*₂ = 5.6 Hz). $^{13}\text{C-NMR}$ (75 MHz, CDCl_3) δ : 116.1 (*d*, $^2J_{\text{C-F}}$ = 21.8 Hz), 123.32, 123.34, 128.6, 129.6 (*d*, $^4J_{\text{C-F}}$ = 3.0 Hz), 135.3, 135.4, 136.9 (*d*, $^3J_{\text{C-F}}$ = 9.0 Hz), 140.0, 142.4, 145.4, 165.6 (*d*, $^1J_{\text{C-F}}$ = 255.8 Hz), 189.1, 190.1.

2-(3-hydroxybenzylidene)-1H-indene-1,3(2H)-dione (10) Yellow solid, Mp 212.0–212.8 °C (Lit.: 212.1–212.8 °C) [31]. IR (ATR) $\bar{\nu}$: 3232, 2898, 2844, 1997,

1717, 1662, 1575, 1452, 1387, 855, 736 cm^{-1} . $^1\text{H-NMR}$ (300 MHz, $\text{DMSO-}d_6$) δ : 7.03 (1H, *d*, *J* = 8.1 Hz), 7.35 (1H, *t*_{ap}, *J* = 7.9 Hz), 7.73 (1H, *s*), 7.83 (1H, *d*, *J* = 7.7 Hz), 7.92–7.99 (4H, *m*), 8.02 (1H, *s*). $^{13}\text{C-NMR}$ (75 MHz, $\text{DMSO-}d_6$) δ : 120.1, 121.2, 123.5, 123.6, 125.9, 129.5, 130.2, 134.4, 136.3, 136.4, 139.9, 142.4, 146.3, 157.8, 188.9, 189.9.

2-(2-hydroxybenzylidene)-1H-indene-1,3(2H)-dione (11) Yellow solid, Mp 182.2–182.5 °C (Lit.: 182.1–182.3 °C) [31]. IR (ATR) $\bar{\nu}$: 3349–2991 (broad band), 1994, 1959, 1713, 1667, 1565, 1457, 1272, 1152, 848, 731 cm^{-1} . $^1\text{H-NMR}$ (300 MHz, $\text{DMSO-}d_6$) δ : 6.90–7.00 (2H, *m*), 7.42–7.47 (1H, *m*), 7.89–7.93 (4H, *m*), 8.31 (1H, *s*), 8.87 (1H, *d*, *J* = 7.9 Hz), 10.85 (1H, *s*). $^{13}\text{C-NMR}$ (75 MHz, $\text{DMSO-}d_6$) δ : 116.4, 119.4, 120.3, 123.3, 123.4, 127.5, 133.6, 136.1, 136.2, 136.5, 139.8, 140.3, 142.2, 160.4, 189.3, 190.4.

Synthesis of C-3 functionalized isobenzofuran-1(3H)-ones

Synthesis of 3-(2-hydroxy-4,4-dimethyl-6-oxo-cyclohexen-1-yl)isobenzofuran-1(3H)-one (12) The phthalaldehydic acid (154 mg, 1.00 mmol), the 5,5-dimethylcyclohexane-1,3-dione (147 mg, 1.00 mmol), and the nanostructured NaNbO_3 catalyst (13.0 mg, 0.0800 mmol) were added to a sealed tube (10 mL). The mixture was irradiated in the microwave reactor at 85 °C with a ramp time of 2 min, medium stirring, and using a closed system for 10 min. The reaction was monitored by thin-layer chromatography. After completion of the reaction, ethyl acetate was added to the reaction mixture followed by simple filtration. The resulting material was recrystallized from ethyl acetate. Compound **12** was obtained in 83% yield (223 mg, 0.830 mmol). The structure of **12** is supported by the following data.

White solid, Mp 211.3–212.1 °C (Lit.: 212.1–213.0 °C) [29]. IR (ATR) $\bar{\nu}$: 2962, 2934, 2884, 2535 (broad band), 1763, 1569, 1382, 1321, 1121, 1059, 942, 738, 694, 613, 574 cm^{-1} . $^1\text{H-NMR}$ (400 MHz, $\text{MeOH-}d_4$) δ : 1.09 (6H, *s*), 2.35 (4H, *s*), 6.70 (1H, *s*), 7.31 (1H, *d*, *J* = 7.6 Hz), 7.50 (1H, *t*, *J* = 7.6 Hz), 7.66 (1H, *t*, *J* = 7.6 Hz), 7.81 (1H, *d*, *J* = 7.6 Hz). $^{13}\text{C-NMR}$ (100 MHz, $\text{MeOH-}d_4$) δ : 28.5, 33.1, 47.9, 76.6, 110.1, 122.6, 125.8, 128.2, 129.5, 135.2, 152.4, 174.2, 188.9.

Synthesis of C-3 functionalized isobenzofuran-1(3H)-ones 13–16 A similar procedure to that described for the

preparation of **12** was utilized to synthesize compounds **13–16**. The structures of these compounds are supported by the following data.

3-(2-hydroxy-5-oxocyclopent-1-enyl)isobenzofuran-1(3H)-one (13) White solid, Mp 206.2–207.1 °C (Lit.: 203.6–205.2 °C) [29]. IR (ATR) $\bar{\nu}$: 2987, 2930, 2370 (broad band), 2366, 2339, 1763, 1648, 1557, 1368, 1281, 1048, 963. $^1\text{H-NMR}$ (200 MHz, $\text{CDCl}_3 + \text{DMSO-}d_6$) δ : 2.27 (4H, brs), 6.07 (1H, s), 7.11 (1H, *d*, $J = 7.2$ Hz), 7.23–7.45 (2H, *m*), 7.62 (1H, *d*, $J = 7.2$ Hz). $^{13}\text{C-NMR}$ (50 MHz, $\text{CDCl}_3 + \text{DMSO-}d_6$) δ : 31.8, 74.5, 112.6, 123.3, 126.0, 127.5, 129.7, 134.9, 150.1, 172.2, 197.3.

2-(3-oxo-1,3-dihydroisobenzofuran-1-yl)-1H-indene-1,3(2H)-dione (14) Brown solid, Mp 214.9–216.3 °C (Lit.: 214.0–215.3 °C) [29]. IR (ATR) $\bar{\nu}$: 3068, 2922, 1770, 1741, 1702, 1266, 1221, 1054 cm^{-1} . $^1\text{H-NMR}$ (400 MHz, $\text{CDCl}_3 + \text{DMSO-}d_6$) δ : 4.12 (1H, *d*, $J = 2.4$ Hz), 6.20 (1H, *d*, $J = 2.4$ Hz), 7.84 (*m*, 8H). $^{13}\text{C-NMR}$ (100 MHz, $\text{CDCl}_3 + \text{DMSO-}d_6$) δ : 55.0, 77.3, 124.2, 123.1, 123.6, 125.3, 125.8, 129.5, 134.4, 136.1, 142.1, 142.5, 147.4, 169.4, 194.9, 196.3.

3-(2-hydroxy-6-oxocyclohex-1-enyl)isobenzofuran-1(3H)-one (15) White solid, Mp 217.6–218.3 °C (Lit.: 217.5–218.0 °C) [29]. IR (ATR) $\bar{\nu}$: 2960, 2917, 2887, 2555 (broad band), 1758, 1565, 1380, 1281, 1056, 1025, 944 cm^{-1} . $^1\text{H-NMR}$ (400 MHz, $\text{DMSO-}d_6$) δ : 1.83–1.91 (2H, *m*), 2.26–2.45 (4H, *m*), 6.59 (1H, s), 7.30 (1H, *d*, $J = 7.6$ Hz), 7.50 (1H, *dd*, $J = 7.6, 7.2$ Hz), 7.65 (1H, *dd*, $J = 7.6, 7.2$ Hz), 7.78 (1H, *d*, $J = 7.6$ Hz). $^{13}\text{C-NMR}$ (100 MHz, $\text{DMSO-}d_6$) δ : 20.1, 32.6, 74.3, 109.1, 121.4, 124.2, 126.5, 128.0, 133.6, 150.7, 170.7, 188.0.

3-(2-hydroxy-4-methyl-6-oxocyclohex-1-enyl)isobenzofuran-1(3H)-one (16) White solid, Mp 190.1–190.5 °C (Lit.: 189.2 – 191.6 °C) [29]. IR (ATR) $\bar{\nu}$: 2960, 2917, 2886, 2565 (broad band), 1757, 1564, 1380, 1281, 1060, 944, 787, 740, 690, 538. $^1\text{H-NMR}$ (400 MHz, $\text{MeOH-}d_4$) δ : 1.08 (3H, *d*, $J = 4.8$ Hz), 2.13–2.55 (5H, *m*), 6.69 (2H, s), 7.31 (1H, *d*, $J = 7.6$ Hz), 7.49 (1H, *dd*, $J = 7.6, 7.2$ Hz), 7.64 (1H, *dd*, $J = 7.6, 7.2$ Hz), 7.81 (1H, *d*, $J = 7.6$ Hz). $^{13}\text{C-NMR}$ (100 MHz, $\text{MeOH-}d_4$) δ : 21.0, 29.5, 42.2, 76.6, 110.8, 122.7, 125.7, 128.2, 129.5, 135.2, 152.4, 174.2, 189.7.

Synthesis of the Meldrum's acid derivatives

5-(4-chlorobenzylidene)-2,2-dimethyl-1,3-dioxane-4,6-dione (17) Meldrum's acid (147 mg, 1.00 mmol), 4-chlorobenzaldehyde (144 mg, 1.00 mmol), and nanostructured NaNbO_3 (13.0 mg, 0.0800 mmol) were added to a sealed tube (10 mL). The reaction mixture was irradiated in the microwave reactor at 85 °C with a ramp time of 2 min, medium agitation, and using a closed system for 5 min. The reaction was monitored by thin-layer chromatography. After the completion of the reaction, dichloromethane was added to the mixture, followed by simple filtration. Compound **17** was obtained as a white solid in 61% yield (161 mg, 0.612 mmol) after recrystallization from dichloromethane–ethanol (1:1 *v v*⁻¹). The structure of **17** is supported by the following data.

Mp 161.1–162.0 °C. IR (ATR) $\bar{\nu}$: 3008, 2991, 2954, 2858, 2011, 1932, 1764, 1730, 1618, 1584, 1403, 1281, 1192, 1030, 933, 822, 793, 417 cm^{-1} . $^1\text{H-NMR}$ (300 MHz, $\text{DMSO-}d_6$) δ : 1.74 (6H, s), 7.56 (2H, *d*, $J = 8.4$ Hz), 8.02 (2H, *d*, $J = 8.4$ Hz), 8.34 (1H, s). $^{13}\text{C-NMR}$ (75 MHz, $\text{DMSO-}d_6$) δ : 27.4, 105.3, 116.6, 129.0, 131.2, 135.1, 138.0, 155.8, 160.1, 162.0.

Synthesis of the Meldrum's acid derivatives 18–21 A similar procedure to that described for the preparation of **17** was utilized to synthesize compounds **18–21**. The structures of these compounds are supported by the following data.

5-(4-bromobenzylidene)-2,2-dimethyl-1,3-dioxane-4,6-dione (18) White solid, Mp 161.1–162.0 °C. IR (ATR) $\bar{\nu}$: 3008, 2946, 2912, 2863, 1932, 1774, 1732, 1490, 1403, 1312, 1264, 1123, 1012, 970, 875, 732, 458 cm^{-1} . $^1\text{H-NMR}$ (300 MHz, $\text{DMSO-}d_6$) δ : 1.74 (6H, s), 7.71 (2H, *d*, $J = 8.4$ Hz), 7.92 (2H, *d*, $J = 8.4$ Hz), 8.33 (1H, s). $^{13}\text{C-NMR}$ (75 MHz, $\text{DMSO-}d_6$) δ : 27.6, 105.1, 116.8, 127.4, 131.5, 131.9, 134.9, 155.8, 159.8, 162.8.

5-(4-fluorobenzylidene)-2,2-dimethyl-1,3-dioxane-4,6-dione (19) White solid, Mp 157.8–158.4 °C. IR (ATR) $\bar{\nu}$: 3012, 2960, 2919, 2858, 1972, 1769, 1732, 1510, 1311, 1200, 1069, 1017, 970, 831, 541, 444 cm^{-1} . $^1\text{H-NMR}$ (300 MHz, $\text{DMSO-}d_6$) δ : 1.74 (6H, s), 7.35 (2H, *t*, $J = 8.7$ Hz), 8.14 (2H, *m*), 8.36 (1H, s). $^{13}\text{C-NMR}$ (75 MHz, $\text{DMSO-}d_6$) δ : 27.4, 105.1, 105.5, 115.5 (*d*, $^4J_{\text{C-F}} = 3.8$ Hz), 116.1 (*d*, $^2J_{\text{C-F}} = 21.8$ Hz), 129.0, 136.6 (*d*,

$^3J_{C-F} = 9.8$ Hz), 156.0, 161.6 (*d*, $^1J_{C-F} = 239.3$ Hz), 164.8.

5-(4-methoxybenzylidene)-2,2-dimethyl-1,3-dioxane-4,6-dione (20) Yellow solid, Mp 122.8–123.5 °C. IR (ATR) $\bar{\nu}$: 2994, 2942, 2844, 1990, 1976, 1709, 1571, 1427, 1370, 1281, 1161, 1015, 930, 835, 795 cm^{-1} . $^1\text{H-NMR}$ (300 MHz, DMSO- d_6) δ : 1.72 (6H, *s*), 3.86 (3H, *s*), 7.07 (2H, *d*, $J = 8.7$ Hz), 8.21 (2H, *d*, $J = 8.7$ Hz), 8.29 (1H, *s*). $^{13}\text{C-NMR}$ (75 MHz, DMSO- d_6) δ : 27.6, 56.4, 104.6, 112.0, 114.9, 125.0, 137.6, 157.2, 160.7, 163.7, 164.4.

2,2-dimethyl-5-(3,4,5-trimethoxybenzylidene)-1,3-dioxane-4,6-dione (21) Orange solid, Mp 157.8–158.9 °C. IR (ATR) $\bar{\nu}$: 3002, 2981, 2950, 2836, 1972, 1713, 1563, 1426, 1394, 1183, 1015, 933, 862, 792 cm^{-1} . $^1\text{H-NMR}$ (300 MHz, DMSO- d_6) δ : 1.73 (6H, *s*), 3.78 (3H, *s*), 3.80 (6H, *s*), 7.67 (2H, *s*), 8.29 (1H, *s*). $^{13}\text{C-NMR}$ (75 MHz, DMSO- d_6) δ : 27.3, 56.6, 60.8, 104.8, 112.7, 114.2, 122.4, 143.0, 152.8, 157.2, 160.4, 163.5.

Synthesis of 3-carboxy coumarin (22)

Meldrum's acid (147 mg, 1.00 mmol), 2-hydroxy benzaldehyde (122 mg, 1.00 mmol), and nanostructured NaNbO_3 (13.0 mg, 0.0800 mmol) were added to a sealed tube (10 mL). The reaction mixture was irradiated in the microwave reactor at 85 °C with a ramp time of 2 min, medium agitation, and using a closed system for 10 min. The reaction was monitored by thin-layer chromatography. After the completion of the reaction, dichloromethane was added to the mixture, followed by simple filtration. Compound **22** was obtained as a white solid in 82% yield (156 mg, 0.821 mmol) after recrystallization from dichloromethane–ethanol (1:1 v v $^{-1}$). The structure of **22** is supported by the following data.

White solid, Mp 190.3–191.5 °C (Lit.: 191.0–192.0 °C) [33]. IR (ATR) $\bar{\nu}$: 3060, 2919, 2778, 1976, 1736, 1672, 1606, 1565, 1416, 1225, 1040, 826, 792, 644, 467 cm^{-1} . $^1\text{H-NMR}$ (300 MHz, DMSO- d_6) δ : 7.35 – 7.42 (2H, *m*), 7.70 (1H, *t*, $J = 7.8$ Hz), 7.88 (1H, *d*, $J = 7.8$ Hz). $^{13}\text{C-NMR}$ (75 MHz, DMSO- d_6) δ : 116.6, 118.4, 118.7, 125.2, 130.7, 134.8, 149.1, 155.0, 157.2, 164.7.

Results and discussion

For the development of a high-performance catalytic process, our initial focus was the synthesis of an original catalyst based on Nb, which had a high capacity to promote condensation reactions of organic compounds. To this end, as shown in Fig. S1, we employed a hydrothermal route inspired by the process reported by Dos Reis to obtain nanostructures based on TiO_2 nanowires with precise control of their properties [42]. Thus, using a commercial niobium oxide, $\text{Nb}_2\text{O}_5 \cdot n\text{H}_2\text{O}$ (supplied by CBMM), as a starting material, NaNbO_3 nanoplates with well-defined and controlled shapes and narrow size distribution could be successfully obtained, as shown in Fig. 1, which depicts the scanning electron microscopy (SEM), scanning transmission electron microscopy (STEM), dark field STEM, and elemental mapping of Nb, O, and Na images for the obtained NaNbO_3 nanoplates. For comparison, the same analyses were carried out for the commercial $\text{Nb}_2\text{O}_5 \cdot n\text{H}_2\text{O}$ (Fig. S2).

First of all, it can clearly be noted that the commercial $\text{Nb}_2\text{O}_5 \cdot n\text{H}_2\text{O}$ catalyst presented typical features of commercial solid oxides (SiO_2 , TiO_2 , CeO_2 , among others) [43, 44], which includes the poor control over shape and size, and no morphological definition (Fig. S2A–G). On the other hand, as depicted in the EDS elemental maps for Nb (red, Fig. S2H) and O (green, Fig. S2I), both Nb and O were uniformly distributed in all $\text{Nb}_2\text{O}_5 \cdot n\text{H}_2\text{O}$ structure without the presence of any other element in its composition, as indicated by the EDS spectra obtained from a set of particles (Fig. S2G). However, as illustrated by the images in Fig. 1, using the hydrothermal method, NaNbO_3 nanoplates displaying well-defined sizes and shapes were obtained, illustrating the robustness of our employed protocol. The obtained nanoplates were 55.7 ± 39.3 nm in width and $> 0.4 \mu\text{m}$ in length, as depicted in the histograms of size distribution (Fig. S3). As observed in the SEM (Fig. 1a), bright field STEM (Fig. 1b), dark field STEM (Fig. 1c), HRTEM (Figs. 1d–f), and EDS elemental mapping of Na (Fig. 1h), Nb (Fig. 1i), and O (Fig. 1j) images, it is observed that the obtained NaNbO_3 structure is comprised by a set of nanoplates superimposed on each other. However, through ultrasound washing and redispersion, it was possible to separate the nanoplates individually and observe their structural, dimensional, and morphological

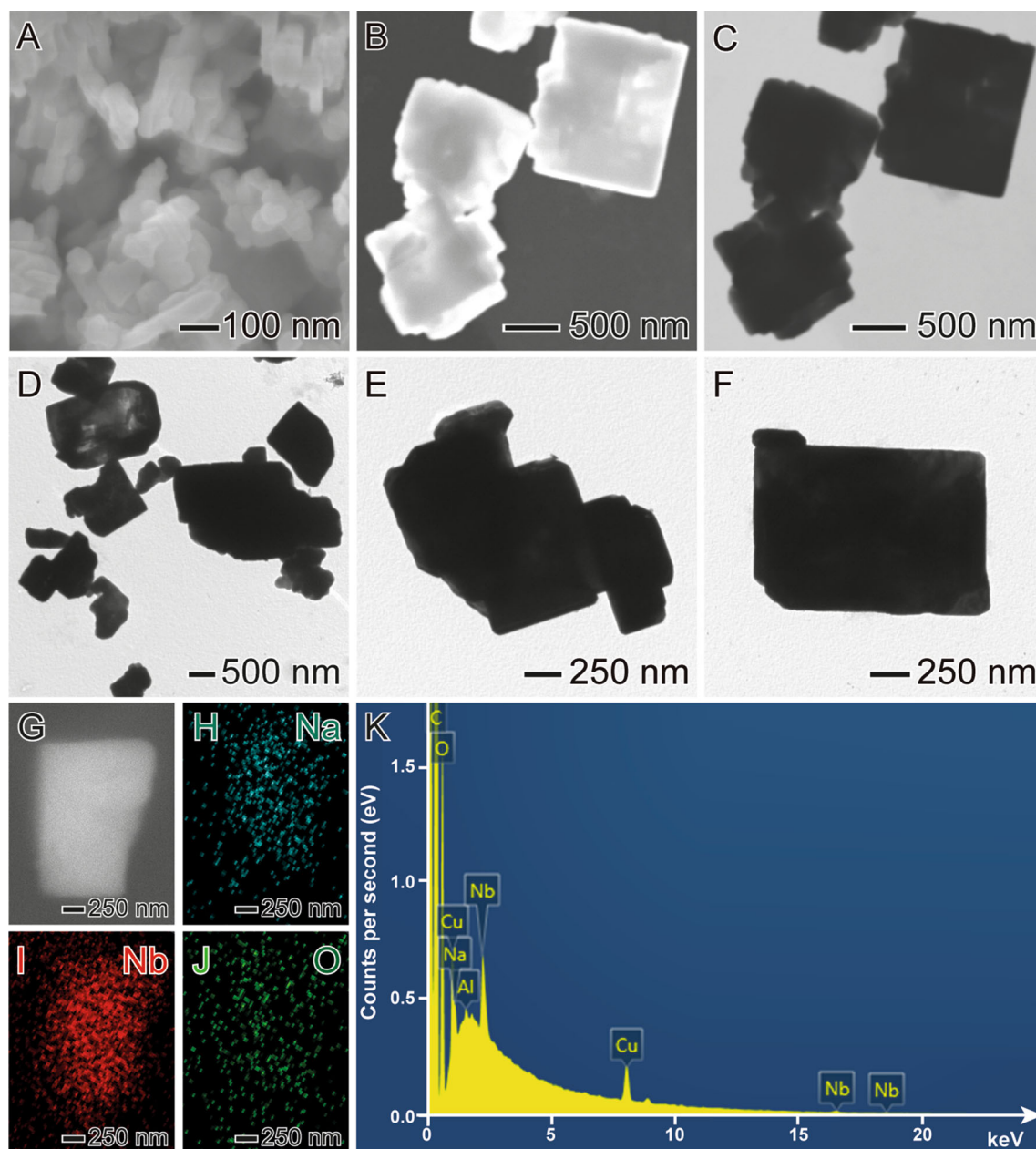


Figure 1 SEM **a**, STEM dark field **b**, STEM bright field **c**, HRTEM **d–f**, EDS elemental mapping **g–j** images, and EDS spectrum **k** for the NaNbO_3 nanoplates.

characteristics. Herein, as shown in Figs. 1h–j, all Na, Nb, and O atoms were uniformly distributed along the entire NaNbO_3 structure indicating the successful combination of these elements in the NaNbO_3 nanoplates, which is consistent with the formation of a solid solution displaying a uniform composition without any elemental segregation throughout the particle length [45].

XRD patterns for the commercial $\text{Nb}_2\text{O}_5 \cdot n\text{H}_2\text{O}$ and the obtained NaNbO_3 nanoplates are shown in

Fig. 2a. Herein, the diffractogram for the commercial $\text{Nb}_2\text{O}_5 \cdot n\text{H}_2\text{O}$ (red curve) presented a typical behavior of mostly amorphous structures with two broad peaks related to N_2O_5 -based phases [46]. On the other hand, the obtained NaNbO_3 nanoplates (black curve) presented a well-defined profile composed of peaks assigned to only NaNbO_3 crystalline phases without any detected impurities, in agreement with the EDS images and spectra (Figs. 1h–k) [22].

Figure 2 XRD patterns **a**, H₂-TPR profiles **b**, CO₂ desorption profiles **c**, and NH₃ desorption profiles **d** for the commercial Nb₂O₅ (red) and the NaNbO₃ nanoplates (black).

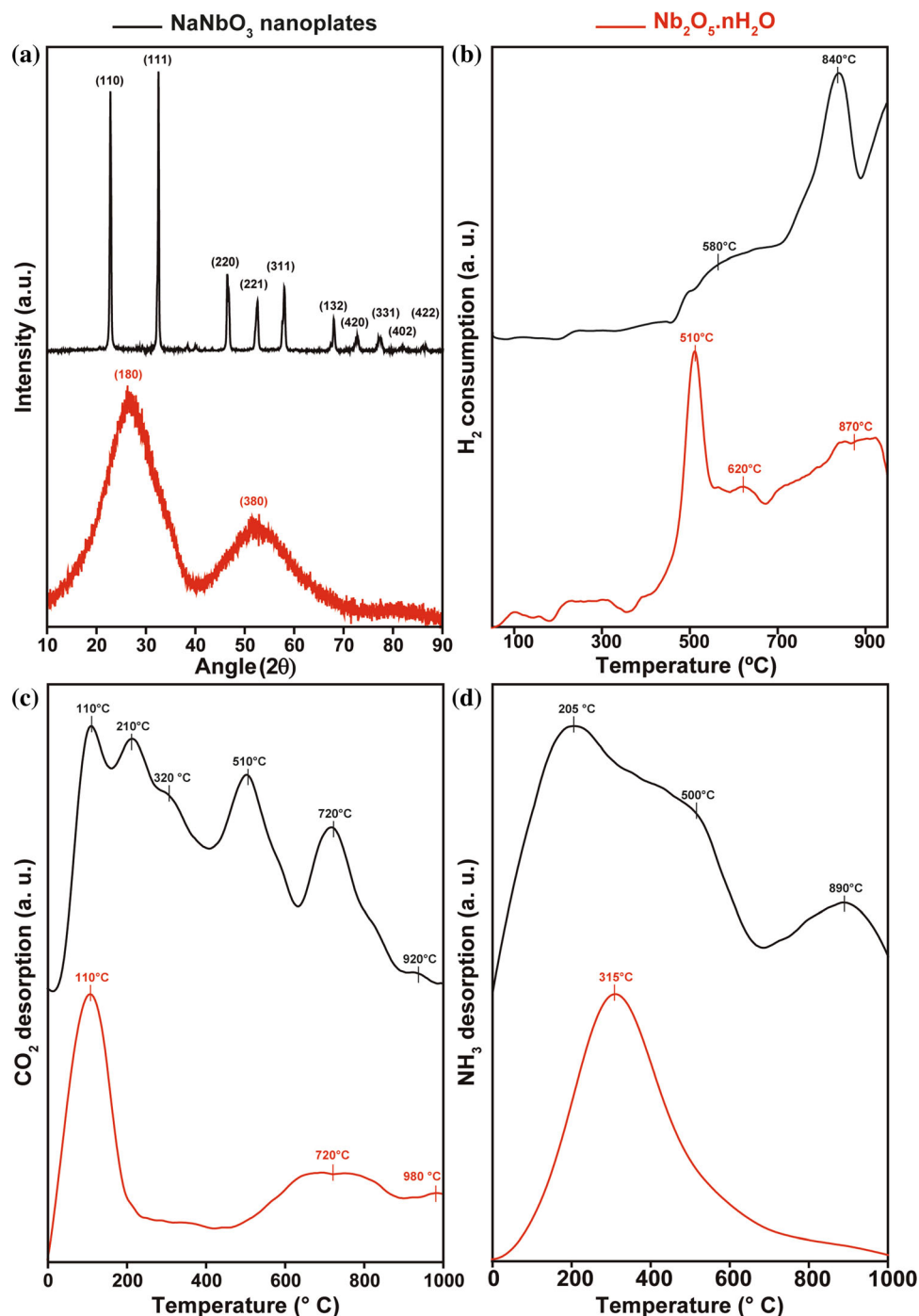


Figure 2b shows the H₂-TPR profiles for the commercial Nb₂O₅·nH₂O and the obtained NaNbO₃ nanoplates. In the profile for the commercial Nb₂O₅·nH₂O, we could observe three peaks of H₂ consumption centered at 510, 620, and 870 °C assigned to the reduction in surface and bulk Nb₂O₅ species [47]. In contrast, in the profile obtained for the NaNbO₃ nanoplates, we could observe only two peaks of H₂

consumption centered at 580 and 840 °C assigned to the reduction in surface and bulk Nb species, respectively. When comparing the two profiles, we can notice a significant increase in the relative intensity of the highest temperature peak in the NaNbO₃ nanoplates, indicating an increase in the amount of oxidizable Nb sites inside and, consequently, in the reduction in oxidizable Nb sites at the

surface. This behavior can be observed if the surface area of the material is decreased during the conversion process from $\text{Nb}_2\text{O}_5 \cdot n\text{H}_2\text{O}$ to NaNbO_3 . Since the conversion is carried out under relatively severe conditions of temperature and pressure, it can lead to the sintering of the starting material, forming a material with less porosity and, consequently, presenting a smaller surface area, as shown in the N_2 physisorption analyses (Table 1) [48–50]. Here, the hydrothermal processing in the presence of NaOH at 150°C of commercial $\text{Nb}_2\text{O}_5 \cdot n\text{H}_2\text{O}$ led to its conversion into a distinct compound, in which Na^+ ions were incorporated into the final structure of the material which, in turn, had an effect similar to a sintering, with a significant reduction in its porosity, as observed in the microscopy images (Figs. 1 and S2). This effect led to a drastic reduction in the porosity and specific surface area of NaNbO_3 nanoplates. However, a surprising behavior in the acidity and surface basicity measured by CO_2 -TPD (Table 1, Fig. 2c) and NH_3 -TPD (Table 1, Fig. 2d) of these materials overcame the effect of the specific surface area in the catalytic tests.

As given in Table 1, NaNbO_3 nanoplates had a greater number of basic sites compared to commercial $\text{Nb}_2\text{O}_5 \cdot n\text{H}_2\text{O}$ through CO_2 -TPD analyses (0.3 and $0.2 \mu\text{mol CO}_2$ per gram of NaNbO_3 and $\text{Nb}_2\text{O}_5 \cdot n\text{H}_2\text{O}$, respectively). However, the inverse tendency was observed in the measurements of the number of acid sites through the NH_3 -TPD analyses, in which NaNbO_3 nanoplates had a number of acid sites of $20.3 \mu\text{mol.g}^{-1}$ and the commercial $\text{Nb}_2\text{O}_5 \cdot n\text{H}_2\text{O}$ had a significantly higher number of acid sites corresponding to $55.9 \mu\text{mol.g}^{-1}$. This effect can be explained based on Wulff's principle, which indicates that the surface properties of a given material are strongly dependent on its morphology [51]. This postulate was verified experimentally and also

theoretically through simulation and computational modeling, which revealed the direct influence on the surface acidity and basicity of nanomaterials with different morphologies [52, 53]. Gianmario Martra [54] published a study based on HRTEM analysis and FTIR spectroscopy, in which the number and the intensity of acidic and basic Lewis sites on the surface of TiO_2 particles with distinct morphologies were determined. In this study, a precise relationship between surface morphology and acidic/basic behavior was successfully established, indicating that high-acid Lewis metallic ions are preferentially exposed in regular surface planes similar to prismatic plates, which corroborates the results observed in Fig. 2D. Here, although the total number of acidic sites of NaNbO_3 nanoplates was significantly lower than commercial $\text{Nb}_2\text{O}_5 \cdot n\text{H}_2\text{O}$ (Table 1), it could be observed that the NH_3 desorption peaks for the nanoplates occurred at higher temperatures (205 , 500 and 890°C). On the other hand, the commercial $\text{Nb}_2\text{O}_5 \cdot n\text{H}_2\text{O}$ sample presented a single NH_3 desorption peak at 315°C , which indicates that the Lewis acid sites present in the nanoplates have a higher intensity than its commercial $\text{Nb}_2\text{O}_5 \cdot n\text{H}_2\text{O}$ counterpart. This property, in turn, has a direct effect on the performances of these materials in catalytic applications, as they are phenomena that can direct specific reaction pathways, being more or less active based on the level of acidity and basicity, considering the type of site required by the application of interest. Here, specifically, we are interested in condensation reactions, which involve an aldehyde adsorption step on the catalyst surface (Figs. 3, 4, 5 and 6). Thus, for this reaction, a catalyst with highly strong acid sites is preferably required. A stronger acidity facilitate the adsorption of the aldehyde on the surface of the catalyst. Due to the differences in the acidity levels of the catalysts in question, differences in catalytic

Table 1 Surface properties of the Nb-based catalysts measured by N_2 physisorption and CO_2 -TPD and NH_3 -TPD

Sample	N_2 physisorption			CO_2 -TPD	NH_3 -TPD
	Surface area ($\text{m}^2 \text{g}^{-1}$)	Average pore diameter (\AA)	Pore volume ($\text{cm}^3 \cdot \text{g}^{-1}$)	CO_2 desorbed ($\mu\text{mol} \cdot \text{g}^{-1}$)	NH_3 desorbed ($\mu\text{mol} \cdot \text{g}^{-1}$)
$\text{Nb}_2\text{O}_5 \cdot n\text{H}_2\text{O}$ commercial	155.6	3.7	0.119	0.2	55.9
NaNbO_3 nanoplates	4.4	12.6	0.014	0.3	20.3

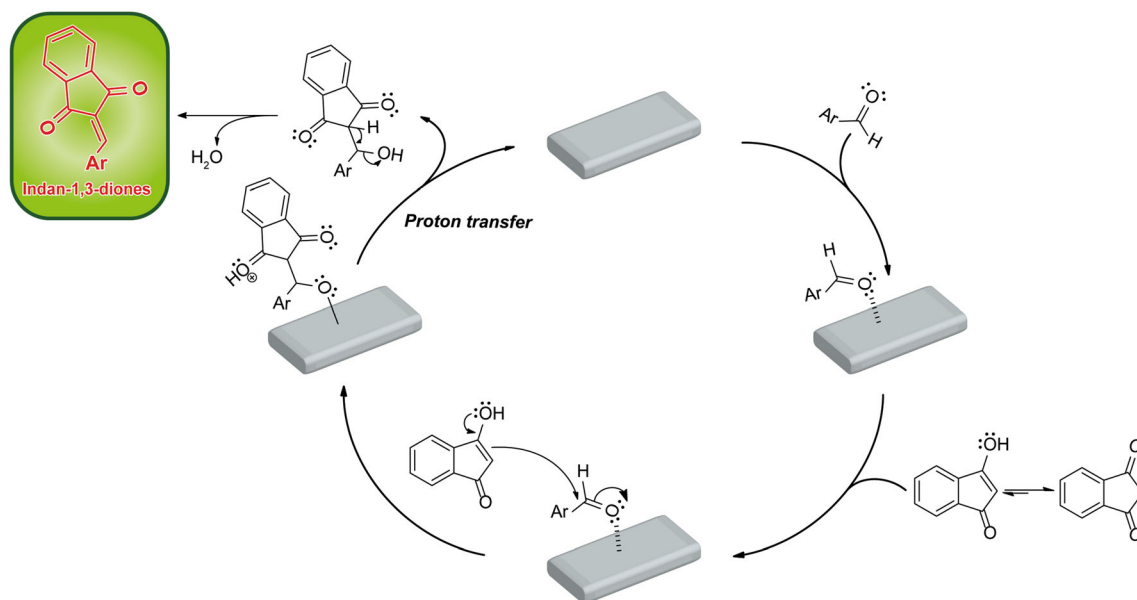


Figure 3 Proposed mechanism for niobium-catalyzed Knoevenagel reaction between indan-1,3-dione and different aldehydes.

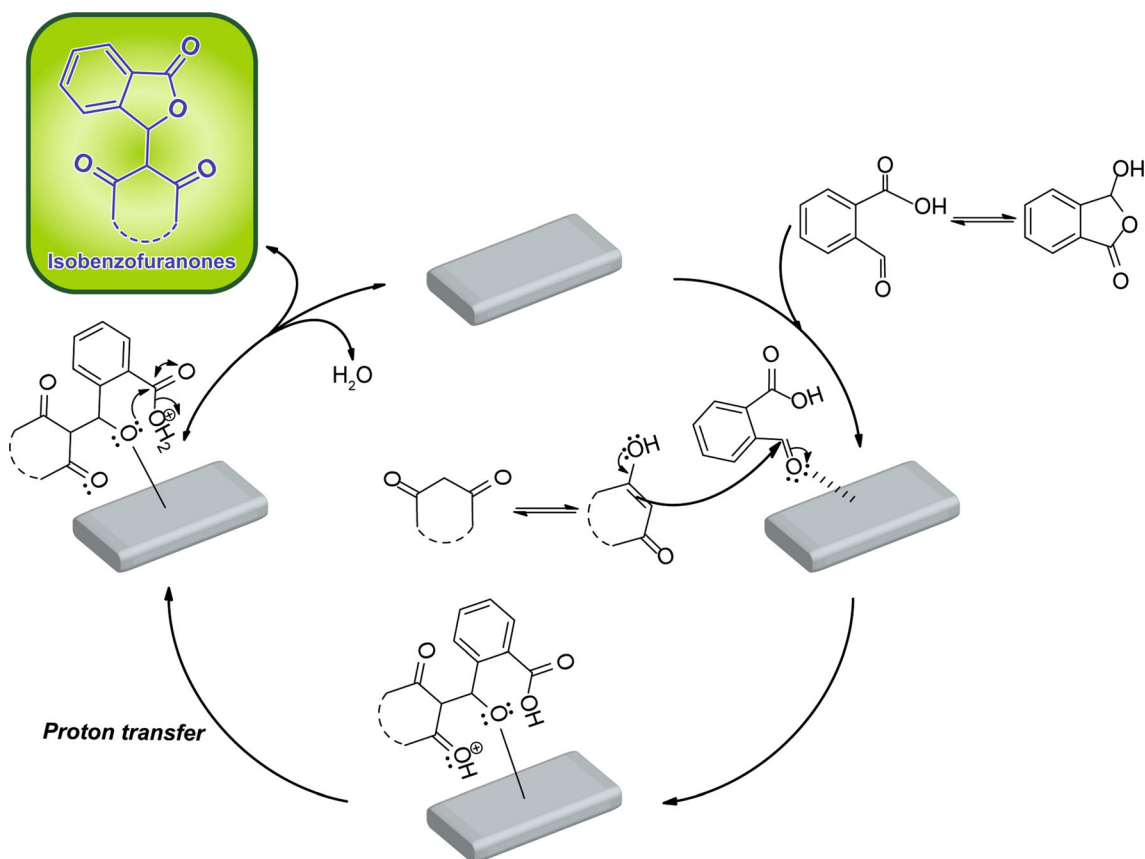


Figure 4 Proposed mechanism for the synthesis of C-3 functionalized isobenzofuran-1(3H)-ones 12-16.

performance were observed, and this parameter was appointed as the predominant among the possible effects in the reactions of interest, such as the specific

surface area. In fact, during the investigation of the condensation reactions discussed ahead, the performance of NaNbO_3 nanostructured as catalysts was

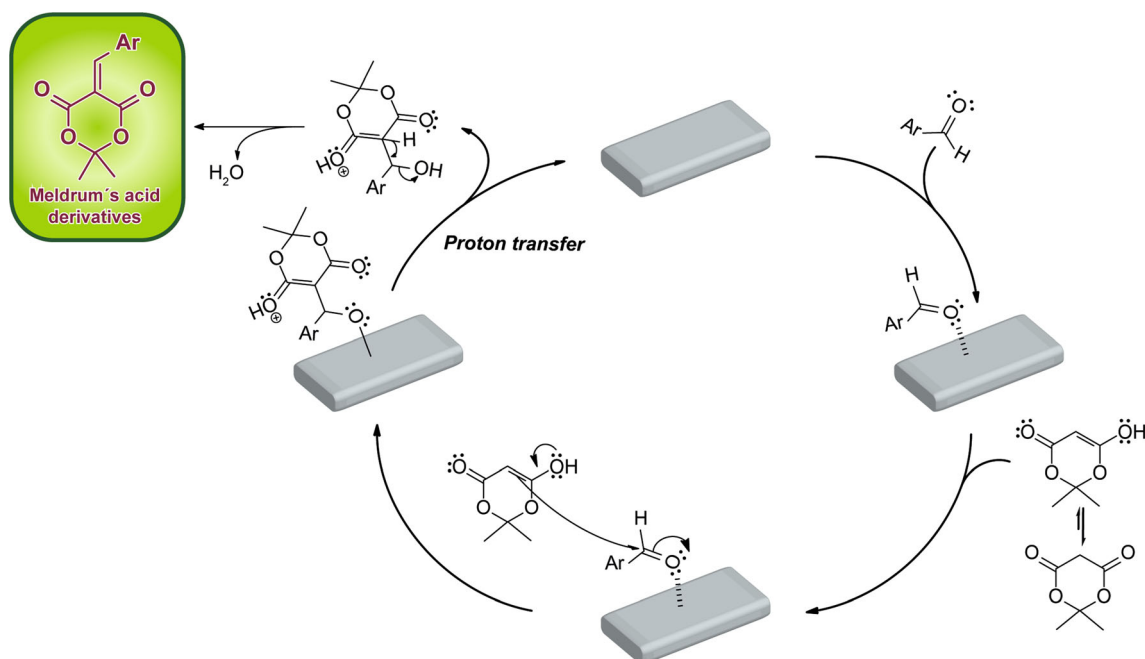
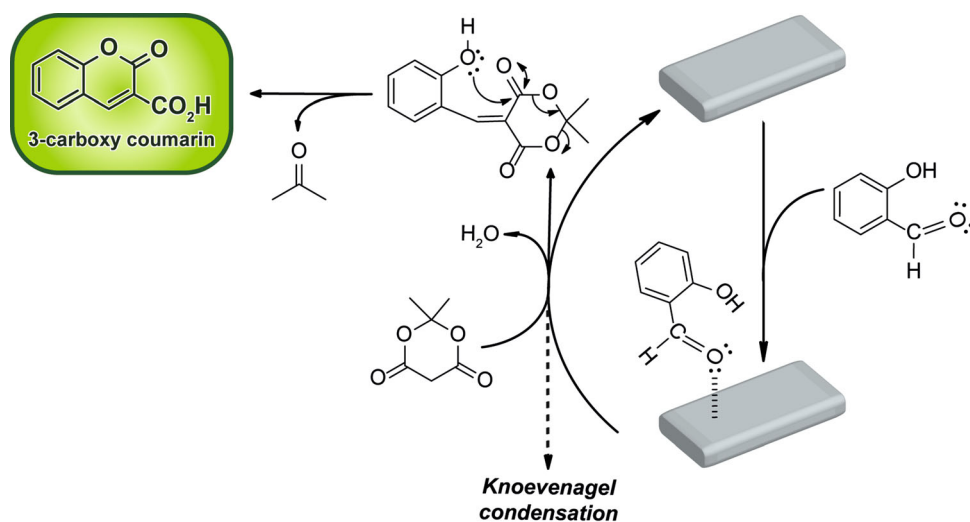


Figure 5 Proposed mechanism for the synthesis of Meldrum's acid derivatives 17–21.

Figure 6 Mechanism proposal for the preparation of **22** from Meldrum's acid and 2-hydroxy benzaldehyde.



superior as compared to the commercial $\text{Nb}_2\text{O}_5 \cdot n\text{H}_2\text{O}$ (which is composed of Nb_2O_5 particles connected). We believed that this fact is related to the intrinsic nature of the materials, being the acidity levels of the catalysts the predominant parameter related to the efficiency of them.

Once obtained, we turned our attention to evaluate the performance of the NaNbO_3 nanostructured in condensation reactions. The first investigated of these processes corresponded to the Knoevenagel condensation between indan-1,3-dione and aldehydes to afford 2-arylidene indan-1,3-diones. The indan-1,3-

dione and its derivatives are valuable synthetic precursors that have been widely applied for the production of dyes [55], semiconductors [56], heterocycles [57, 58], and pharmaceuticals [59]. Indan-1,3-dione derivatives present several biological activities such as antitumoral [60], anticoagulant [61], anti-inflammatory [62, 63], neuroprotective [64], and antimicrobial [65]. Besides, compounds presenting the indan-1,3-dione core has been isolated from nature [66, 67] and displaying important bioactivities [68, 69]. Our research group has been interested in the chemistry as well as biological profile of indan-1,3-

dione derivatives. Recently, we have described the preparation and antiviral evaluation of 2-arylidene indan-1,3-diones [32]. In view of the importance of indan-1,3-dione derivatives as building blocks as well as their biological profile, the development of methodologies to prepare these derivatives is of relevance. Herein, we found that NaNbO_3 nanostructured is a useful catalyst to prepare 2-arylidene indan-1,3-diones via Knoevenagel condensation between indan-1,3-dione and several aldehydes. After optimization of the reaction conditions, it was found that the indan-1,3-dione derivatives could be obtained with good yields by running the reactions under microwave irradiation and using 8 mol% of catalyst (Table 2).

As given in Table 2, indandione derivatives with different substitution patterns for the aromatic ring of the arylidene portion were prepared in only 10 min under microwave irradiation conditions. The reactions were conducted without the presence of solvent and compounds containing electron-withdrawing and electron-donating groups attached to the arylidene portion were obtained with synthetic useful yields. All the derivatives were purified via recrystallization procedures. For the sake of completeness, spectroscopic data (IR and NMR) which confirmed the identity of the compounds are provided.

To demonstrate the catalytic effect of NaNbO_3 , a reaction between 4-chloro benzene and indan-1,3-dione were carried in the absence of the catalyst. The corresponding 2-arylidene indan-1,3-dione derivative (compound **1** in Table 2) was obtained with lower yield (57%) and higher reaction time (45 min).

The reusability of NaNbO_3 catalyst was investigated. The reaction between 4-chloro benzaldehyde and indan-1,3-dione was used in the recycling study, and the results are given in Table 3. After each run, the catalyst was separated by adding dichloromethane to the reaction mixture which, in turn, was submitted to centrifugation. The recovered catalyst was dried and then reused. As can be seen, the efficiency of the catalyst was not diminished after three cycles, being the product **1** obtained with significant yield in each cycle.

Even though a mechanistic investigation was not carried out, a proposed mechanism for the NaNbO_3 -catalyzed Knoevenagel condensation for the preparation of 2-arylidene indan-1,3-diones is shown in Fig. 3.

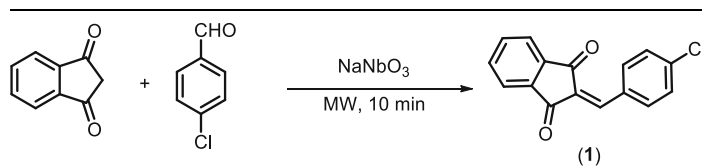
Another class of compounds that have attracted the attention of several research groups, including ourselves [29–41, 46–48], is the isobenzofuran-1(3*H*)-ones. They present as common structural feature a γ -lactone fragment fused to a benzene ring. Isobenzofuranones are useful building blocks in organic

Table 2 NaNbO_3 -catalyzed Knoevenagel condensation for the preparation of 2-arylidene indan-1,3-diones

Compound	Ar	Yield (%) ^a
1	4-chlorophenyl	70
2	4-nitrophenyl	79
3	4-bromophenyl	74
4	4-methoxyphenyl	70
5	4-hydroxyphenyl	74
6	4-hydroxy-3-methoxyphenyl	75
7	phenyl	57
8	3,4,5-trimethoxyphenyl	81
9	4-fluorophenyl	75
10	3-hydroxyphenyl	65
11	2-hydroxyphenyl	78

^a The reactions were run using aldehyde (1.00 mmol) and indan-1,3-dione (1.00 mmol). The yields were determined after purification of the compounds by recrystallization

Table 3 Results of the reuse of NaNbO_3 catalyst in the reaction involving indan-1,3-dione and 4-chloro benzaldehyde



Cycle	Amount of catalyst (g)	Yield (%) ^a
1	0.0132	74
2	0.0124	70
3	0.0115	72

Reactions were run utilizing 4-chlorobenzaldehyde (1.00 mmol) and indan-1,3-dione (1.00 mmol)

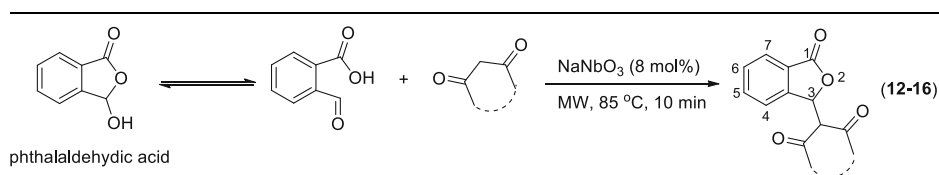
^a The yields were determined after recrystallization of the product 1

synthesis (as in the Houser annulation) [70] and display important biological activities [29]. In view of their relevance, the development of synthetic methodologies to prepare them is of potential interest. In the present investigation, a series of C-3 functionalized isobenzofuran-1(3*H*)-ones was obtained via the NaNbO_3 -catalyzed condensation

reactions involving 2-carboxy benzaldehyde (phthalaldehydic acid) and different β -diketones (Table 4).

The functionalized isobenzofuran-1(3*H*)-ones were obtained with satisfactory yields ranging from 63 to 83% after 10 min of reaction. The conditions used to run the reactions were identical to that used in the preparation of compounds 1–11. The structure of

Table 4 Preparation of C-3 functionalized isobenzofuran-1(3*H*)-ones via niobium-catalyzed condensation reactions between phthalaldehydic acid and β -diketones



Compound	Yield (%) ^a
	83
	63
	69
	63
	71

Reactions were carried out using 1.00 mmol of phthalaldehydic acid and 1.00 mmol of β -diketone

^aThe yields were calculated after purification of the compounds by recrystallization

isobenzofuranones **12–16** were confirmed based on IR and NMR spectroscopic data.

Running the reaction between phthalaldehydic acid and 5,5-dimethyl-1,3-cyclohexadione (dime-done) without the presence of the catalyst resulted in the formation of compound **12** in 59% after 40 min of reaction. This fact demonstrate the catalytic effect of NaNbO_3 in the reactions involved in the synthesis of C-3 functionalized isobenzofuran-1(3*H*)-ones.

The reaction involved in the preparation of isobenzofuranone **12** was chosen to investigate the possibility of catalyst reuse. The results in Table 5 demonstrate that the catalyst can be reused without significant loss of performance.

Figure 4 shows the mechanistic proposal for the formation of C-3 functionalized isobenzofuran-1(3*H*)-ones in the presence of the NaNbO_3 catalyst.

The use of NaNbO_3 nanoplates as catalyst was also demonstrated in the preparation of Meldrum's acid derivatives bearing arylidene functionalities as given in Table 6.

The series of Meldrum's acid derivatives were obtained with yields ranging from 61 to 90% and within 5–10 min and had their structures confirmed by IR and NMR spectroscopies. When the reaction for the preparation of compound **17** was run in the absence of the catalyst, the time was six times longer (30 min), and the product yield after recrystallization significantly decreased (only 32%). The same reaction was used to investigate the reutilization of the NaNbO_3 catalyst, and the results are shown in Table 7. As can be observed, the catalyst can be reused without substantial decrease in activity.

It is very likely that the mechanism involved in the synthesis of Meldrum's acid derivatives (Fig. S4) is similar to the one proposed for the preparation of 2-arylidene indan-1,3-diones. Meldrum's acid derivatives are very important compounds in organic synthesis since they can react with several nucleophiles and electrophiles giving rise to several important organic compounds that are useful in the context preparation of, for example, pharmaceuticals [71].

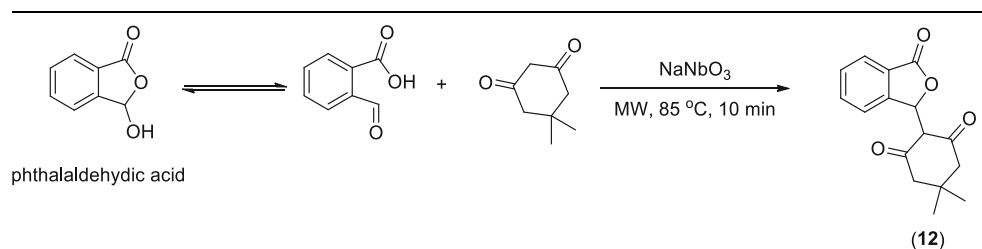
As one last transformation in which the NaNbO_3 herein described was utilized is related to the preparation of a carboxy coumarin. Within this context, a mixture of Meldrum's acid and 2-hydroxy benzaldehyde was microwave irradiated for 10 min in the presence of NaNbO_3 which led to the formation of coumarin **22**, which was obtained in good 82% yield. Figure 6 shows the mechanism proposal for the formation of compound **22**.

Coumarin is a privileged scaffold that is very useful in the design and development of bioactive compounds.[72–74].

Conclusion

In summary, it was demonstrated that a well-defined NaNbO_3 catalyst could be obtained from $\text{Nb}_2\text{O}_5 \cdot n\text{H}_2\text{O}$ via a hydrothermal process. The NaNbO_3 is an efficient catalyst in condensation reactions used for the preparation of indan-1,3-diones, isobenzofuranones, and Meldrum's acid derivatives. A carboxy coumarin was also synthesized by means of a condensation reaction between Meldrum's acid and

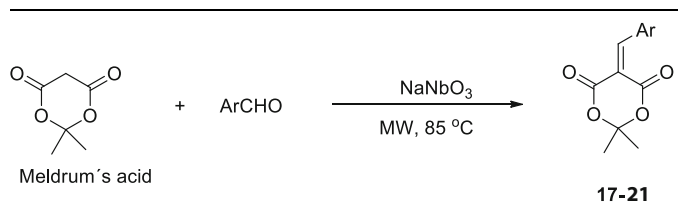
Table 5 Results of the reuse of NaNbO_3 catalyst in the reaction involving phthalaldehydic acid and dime-done



Cycle	Amount of catalyst (g)	Yield (%) ^a
1	0.0132	83
2	0.0124	81
3	0.0105	79

Reactions were carried out with phthalaldehydic acid (1.00 mmol) and dime-done (1.00 mmol)

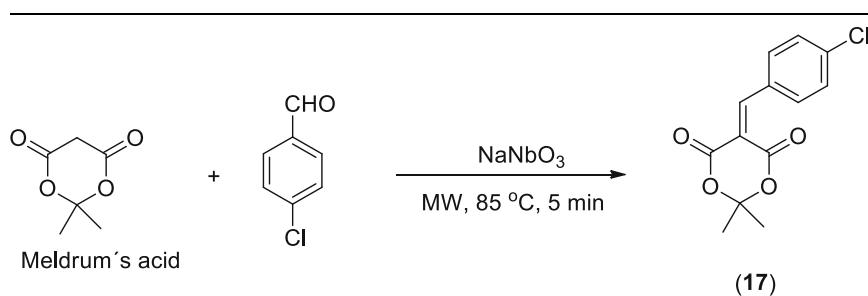
^a The yields were determined after recrystallization of the product

Table 6 NaNbO₃-catalyzed reaction involved in the preparation of Meldrum's acid derivatives


Compound	Ar	Reaction time (min)	Yield (%) ^a
17	4-chlorophenyl	5	61
18	4-bromophenyl	5	71
19	4-fluorophenyl	10	74
20	4-methoxyphenyl	10	87
21	3,4,5-trimethoxyphenyl	10	90

The reactions were run with aldehyde (1.00 mmol) and Meldrum's acid (1.00 mmol)

^a The yields were determined after purification of the compounds by recrystallization

Table 7 Preparation of compound 17 and results of the catalyst reuse experiments


Cycle	Amount of catalyst (g)	Yield (%) ^a
1	0.0132	61
2	0,0115	62
3	0,0102	59

Reactions were run with Meldrum's acid (1.00 mmol) and 4-chloro benzaldehyde (1.00 mmol)

^aYields obtained after recrystallization

2-carboxy benzaldehyde. All of these compounds could be successfully obtained in condensation reactions in which solvent was not used. Another important feature is that the compounds could be purified by simple recrystallization procedures. Finally, the reusability of the catalyst was demonstrated in the condensation reactions.

Acknowledgements

We are grateful to Conselho Nacional de Desenvolvimento Científico e Tecnológico (CNPq), Fundação de Amparo à Pesquisa do Estado do Rio de Janeiro (FAPERJ), Fundação de Amparo à Pesquisa do Estado de Minas Gerais (FAPEMIG), and

Coordenação de Aperfeiçoamento de Pessoal de Nível Superior (CAPES). T.S.R. thanks FAPERJ (Grant number: E-26/201.431/2021) for the financial support. F.A.S. thanks FAPERJ for his fellowship. We are also grateful to the Center of Multidisciplinary Research (UFRJ-Caxias Campus) for the access to the electron microscopy facilities.

Supplementary Information: The online version contains supplementary material available at <http://doi.org/10.1007/s10853-021-06725-0>.

References

- [1] Silveira JW, Resende M (2020) Competition in the international niobium market: a residual demand approach. *Resour Policy* 65:101564. <https://doi.org/10.1016/j.resourpol.2019.101564>
- [2] Paquet N, Indiketi N, Dalencourt C et al (2019) Toxicity of tailing leachates from a niobium mine toward three aquatic organisms. *Ecotoxicol Environ Saf* 176:355–363. <https://doi.org/10.1016/j.ecoenv.2019.03.065>
- [3] Bai Y, Deng Y, Zheng Y et al (2016) Characterization, corrosion behavior, cellular response and in vivo bone tissue compatibility of titanium–niobium alloy with low Young's modulus. *Mater Sci Eng C* 59:565–576. <https://doi.org/10.1016/j.msec.2015.10.062>
- [4] Vilaplana J, Romaguera C (1998) New developments in jewellery and dental materials. *Contact Dermat* 39:55–57. <https://doi.org/10.1111/j.1600-0536.1998.tb05832.x>
- [5] Nowak I, Ziolk M (1999) Niobium compounds: preparation, characterization, and application in heterogeneous catalysis. *Chem Rev* 99:3603–3624. <https://doi.org/10.1021/cr9800208>
- [6] Ziolk M, Sobczak I (2017) The role of niobium component in heterogeneous catalysts. *Catal Today* 285:211–225. <https://doi.org/10.1016/j.cattod.2016.12.013>
- [7] Nico C, Monteiro T, Graça MPF (2016) Niobium oxides and niobates physical properties: review and prospects. *Prog Mater Sci* 80:1–37. <https://doi.org/10.1016/j.pmatsci.2016.02.001>
- [8] do Prado NT, Oliveira LCA (2017) Nanostructured niobium oxide synthesized by a new route using hydrothermal treatment: high efficiency in oxidation reactions. *Appl Catal B Environ* 205:481–488. <https://doi.org/10.1016/j.apcatb.2016.12.067>
- [9] Sieber I, Hildebrand H, Friedrich A, Schmuki P (2005) Formation of self-organized niobium porous oxide on niobium. *Electrochem Commun* 7:97–100. <https://doi.org/10.1016/j.elecom.2004.11.012>
- [10] Zhang P, Wang M, Wang J et al (2018) Facile synthesis and characterization of low crystalline Nb₂O₅ ultrafine nanoparticles as a new efficient photocatalyst. *J Non Cryst Solids* 500:371–376. <https://doi.org/10.1016/j.jnoncrsol.2018.08.026>
- [11] Shiratori Y, Magrez A, Dornseiffer J et al (2005) Polymorphism in micro-, submicro-, and nanocrystalline NaNbO₃. *J Phys Chem B* 109:20122–20130. <https://doi.org/10.1021/jp052974p>
- [12] Jia Y, Zhong M, Yang F et al (2020) Theoretical and experimental study on exciton properties of TT-, T-, and H-Nb₂O₅. *J Phys Chem C* 124:15066–15075. <https://doi.org/10.1021/acs.jpcc.0c04202>
- [13] Sathasivam S, Williamson BAD, Althabaiti SA et al (2017) Chemical vapor deposition synthesis and optical properties of Nb₂O₅ thin films with hybrid functional theoretical insight into the band structure and band gaps. *ACS Appl Mater Interfaces* 9:18031–18038. <https://doi.org/10.1021/acsami.7b00907>
- [14] Asencios YJO, Quijo MV, Marcos FCF et al (2019) Photocatalytic activity of Nb heterostructure (NaNbO₃/Na₂Nb₄O₁₁) and Nb/clay materials in the degradation of organic compounds. *Sol Energy* 194:37–46. <https://doi.org/10.1016/j.solener.2019.10.005>
- [15] Sures D, Segado M, Bo C, Nyman M (2018) Alkali-driven disassembly and reassembly of molecular niobium oxide in water. *J Am Chem Soc* 140:10803–10813. <https://doi.org/10.1021/jacs.8b05015>
- [16] Zhou C, Shi R, Waterhouse GIN, Zhang T (2020) Recent advances in niobium-based semiconductors for solar hydrogen production. *Coord Chem Rev* 419:213399. <https://doi.org/10.1016/j.ccr.2020.213399>
- [17] Ji S, Liu H, Sang Y et al (2014) Synthesis, structure, and piezoelectric properties of ferroelectric and antiferroelectric NaNbO₃ nanostructures. *CrystEngComm* 16:7598–7604. <https://doi.org/10.1039/C4CE01116C>
- [18] Pan Z, Yao L, Ge G et al (2018) High-performance capacitors based on NaNbO₃ nanowires/poly(vinylidene fluoride) nanocomposites. *J Mater Chem A* 6:14614–14622. <https://doi.org/10.1039/C8TA03084G>
- [19] Farooq U, Phul R, Alshehri SM et al (2019) Electrocatalytic and enhanced photocatalytic applications of sodium niobate nanoparticles developed by citrate precursor route. *Sci Rep* 9:4488. <https://doi.org/10.1038/s41598-019-40745-w>
- [20] Yang F, Zhang Q, Zhang L et al (2019) Facile synthesis of highly efficient Pt/N-rGO/N-NaNbO₃ nanorods toward photocatalytic hydrogen production. *Appl Catal B Environ* 257:117901. <https://doi.org/10.1016/j.apcatb.2019.117901>
- [21] Yang F, Zhang Q, Zhang J et al (2020) Embedding Pt nanoparticles at the interface of CdS/NaNbO₃ nanorods heterojunction with bridge design for superior Z-Scheme photocatalytic hydrogen evolution. *Appl Catal B Environ* 278:119290. <https://doi.org/10.1016/j.apcatb.2020.119290>
- [22] You H, Wu Z, Wang L et al (2018) Highly efficient pyro-catalysis of pyroelectric NaNbO₃ shape-controllable nanoparticles for room-temperature dye decomposition. *Chemosphere* 199:531–537. <https://doi.org/10.1016/j.chemosphere.2018.02.059>
- [23] Liu Q, Zhang L, Chai Y, Dai W-L (2017) Facile fabrication and mechanism of single-crystal sodium niobate

- photocatalyst: insight into the structure features influence on photocatalytic performance for H₂ evolution. *J Phys Chem C* 121:25898–25907. <https://doi.org/10.1021/acs.jpcc.7b08819>
- [24] Kumar D, Singh S, Khare N (2018) Plasmonic Ag nanoparticles decorated NaNbO₃ nanorods for efficient photoelectrochemical water splitting. *Int J Hydrog Energy* 43:8198–8205. <https://doi.org/10.1016/j.ijhydene.2018.03.075>
- [25] Wang S, Wu Z, Chen J et al (2019) Lead-free sodium niobate nanowires with strong piezo-catalysis for dye wastewater degradation. *Ceram Int* 45:11703–11708. <https://doi.org/10.1016/j.ceramint.2019.03.045>
- [26] Chen W, Hu Y, Ba M (2018) Surface interaction between cubic phase NaNbO₃ nanoflowers and Ru nanoparticles for enhancing visible-light driven photosensitized photocatalysis. *Appl Surf Sci* 435:483–493. <https://doi.org/10.1016/j.apsusc.2017.11.115>
- [27] Pires DAT, Guedes IA, Pereira WL et al (2021) Isobenzofuran-1(3H)-ones as new tyrosinase inhibitors: biological activity and interaction studies by molecular docking and NMR. *Biochim Biophys Acta—Proteins Proteomics* 1869:140580. <https://doi.org/10.1016/j.bbapap.2020.140580>
- [28] Ribeiro IML, Pereira WL, Nogueira LB et al (2020) Neuroprotective effect of isobenzofuranones on hydrogen peroxide-mediated redox imbalance in primary cultures of hippocampal neurons. *Braz Arch Biol Technol*. <https://doi.org/10.1590/1678-4324-2020190072>
- [29] Teixeira R, Bressan G, Pereira W et al (2013) Synthesis and antiproliferative activity of C-3 functionalized isobenzofuran-1(3H)-ones. *Molecules* 18:1881–1896. <https://doi.org/10.3390/molecules18021881>
- [30] Teixeira RR, Pereira WL, Tomaz DC et al (2013) Synthetic analogues of the natural compound cryphonectric acid interfere with photosynthetic machinery through two different mechanisms. *J Agric Food Chem* 61:5540–5549. <https://doi.org/10.1021/jf400698j>
- [31] Andrezza Costa MC, Miguel Castro Ferreira M, Teixeira RR et al (2021) Synthesis, biological activity, and four-dimensional quantitative structure–activity analysis of 2-arylidene indan-1,3-dione derivatives tested against *Daphnia magna*. *SAR QSAR Environ Res* 32:133–150. <https://doi.org/10.1080/1062936X.2020.1866070>
- [32] da Oliveira AFC, de Souza APM, de Oliveira AS et al (2018) Zirconium catalyzed synthesis of 2-arylidene Indan-1,3-diones and evaluation of their inhibitory activity against NS2B-NS3 WNV protease. *Eur J Med Chem* 149:98–109. <https://doi.org/10.1016/j.ejmech.2018.02.037>
- [33] Pereira JL, Teixeira RR, Guilardi S et al (2012) 6-Methoxyisobenzofuran-1(3H)-one. *Acta Cryst Sect* 68:o2995. <https://doi.org/10.1107/S1600536812039074>
- [34] dos Reis TA, Teixeira RR, Ribeiro IML et al (2020) Association of electroanalytical and spectrophotometric methods to evaluate the antioxidant activity of isobenzofuranone in primary cultures of hippocampal neurons. *Toxicol Vitro* 68:104970. <https://doi.org/10.1016/j.tiv.2020.104970>
- [35] Rodrigues MP, Tomaz DC, Ângelo de Souza L et al (2019) Synthesis of cinnamic acid derivatives and leishmanicidal activity against *Leishmania braziliensis*. *Eur J Med Chem* 183:111688. <https://doi.org/10.1016/j.ejmech.2019.111688>
- [36] de Oliveira AS, Gazolla PAR, da Oliveira AFC et al (2019) Discovery of novel West Nile Virus protease inhibitor based on isobenzonafuranone and triazolic derivatives of eugenol and indan-1,3-dione scaffolds. *PLoS ONE* 14:e0223017. <https://doi.org/10.1371/journal.pone.0223017>
- [37] Pires DAT, Pereira WL, Teixeira RR et al (2016) Nuclear magnetic resonance (NMR), infrared (IR) and mass spectrometry (MS) study of keto-enol tautomerism of isobenzofuran-1(3H)-one derivatives. *J Mol Struct* 1113:146–152. <https://doi.org/10.1016/j.molstruc.2016.02.015>
- [38] da Silva Maia AF, Siqueira RP, de Oliveira FM et al (2016) Synthesis, molecular properties prediction and cytotoxic screening of 3-(2-aryl-2-oxoethyl)isobenzofuran-1(3H)-ones. *Bioorg Med Chem Lett* 26:2810–2816. <https://doi.org/10.1016/j.bmcl.2016.04.065>
- [39] Franca EF, Guilardi S, Paixão DA et al (2016) Centrosymmetric resonance-assisted intermolecular hydrogen bonding chains in the enol form of β-diketone: crystal structure and theoretical study. *J Mol Graph Model* 68:106–113. <https://doi.org/10.1016/j.jmkgm.2016.06.004>
- [40] Pereira W, de Souza VR, Mariotini-Moura C et al (2015) The Antileishmanial Potential of C-3 Functionalized Isobenzofuranones against *Leishmania (Leishmania) Infantum* Chagasi. *Molecules* 20:22435–22444. <https://doi.org/10.3390/molecules201219857>
- [41] Teixeira RR, Pereira JL, Da Silva SF et al (2014) Synthesis, characterization and phytotoxic activity of hydroxylated isobenzofuran-1(3H)-ones. *J Mol Struct* 1061:61–68. <https://doi.org/10.1016/j.molstruc.2013.12.059>
- [42] dos Reis FVE, Antonin VS, Hammer P et al (2015) Carbon-supported TiO₂-Au hybrids as catalysts for the electrogeneration of hydrogen peroxide: investigating the effect of TiO₂ shape. *J Catal* 326:100–106. <https://doi.org/10.1016/j.jcat.2015.04.007>
- [43] Rodrigues TS, eSilva FA, Candido EG et al (2019) Ethanol steam reforming: understanding changes in the activity and stability of Rh/M_xO_y catalysts as function of the support. *J Mater Sci* 54:11400–11416. <https://doi.org/10.1007/s10853-019-03660-z>
- [44] Gualteros JAD, Garcia MAS, da Silva AGM et al (2019) Synthesis of highly dispersed gold nanoparticles on Al₂O₃,

- SiO₂, and TiO₂ for the solvent-free oxidation of benzyl alcohol under low metal loadings. *J Mater Sci* 54:238–251. <https://doi.org/10.1007/s10853-018-2827-x>
- [45] Liu Q, Chai Y, Zhang L et al (2017) Highly efficient Pt/NaNbO₃ nanowire photocatalyst: its morphology effect and application in water purification and H₂ production. *Appl Catal B Environ* 205:505–513. <https://doi.org/10.1016/j.apcatt.2016.12.065>
- [46] Zhang J, Jiang T, Mai Y et al (2019) Selective catalytic oxidation of sulfides to sulfoxides or sulfones over amorphous Nb₂O₅/AC catalysts in aqueous phase at room temperature. *Catal Commun* 127:10–14. <https://doi.org/10.1016/j.catcom.2019.04.013>
- [47] Silva LPC, Freitas MM, Terra LE et al (2020) Preparation of CuO/ZnO/Nb₂O₅ catalyst for the water-gas shift reaction. *Catal Today* 344:59–65. <https://doi.org/10.1016/j.cattod.2018.10.028>
- [48] Leal Marchena C, Saux C, Dinamarca R et al (2016) Alkaline niobates ANbO₃ (A = Li, Na, K) as heterogeneous catalysts for dipropyl sulfide oxidation. *RSC Adv* 6:102015–102022. <https://doi.org/10.1039/C6RA21749D>
- [49] Pecchi G, Cabrera B, Buljan A et al (2013) Catalytic oxidation of soot over alkaline niobates. *J Alloys Compd* 551:255–261. <https://doi.org/10.1016/j.jallcom.2012.10.015>
- [50] Baeissa ES (2016) Photocatalytic degradation of malachite green dye using Au/NaNbO₃ nanoparticles. *J Alloys Compd* 672:564–570. <https://doi.org/10.1016/j.jallcom.2016.02.024>
- [51] Wulff G (1901) XXV. Zur Frage der Geschwindigkeit des Wachstums und der Auflösung der Krystallflächen. *Zeitschrift für Krist - Cryst Mater* 34: 449–530. Doi: <https://doi.org/10.1524/zkri.1901.34.1.449>
- [52] He B, Wang J, Ma D et al (2018) Interaction of Pd single atoms with different CeO₂ crystal planes: a first-principles study. *Appl Surf Sci* 433:1036–1048. <https://doi.org/10.1016/j.apsusc.2017.10.134>
- [53] Wang W, Xiong Z, He W et al (2021) Influence of thiourea modification on the NH₃-SCR activity of CeO₂: Simultaneous tuning morphology and surface acidity. *J Energy Inst* 98:322–333. <https://doi.org/10.1016/j.joei.2021.07.009>
- [54] Martra G (2000) Lewis acid and base sites at the surface of microcrystalline TiO₂ anatase: relationships between surface morphology and chemical behaviour. *Appl Catal A Gen* 200:275–285. [https://doi.org/10.1016/S0926-860X\(00\)00641-4](https://doi.org/10.1016/S0926-860X(00)00641-4)
- [55] Matsui M, Kimura R, Kubota Y et al (2017) Application of indoline dyes having a carboxylated 1,3-indandione ring linked with thienyl or hexylthienyl ring to dye-sensitized solar cells. *Dye Pigment* 147:50–55. <https://doi.org/10.1016/j.dyepig.2017.07.009>
- [56] Du T, Gao R, Deng Y et al (2020) Indandione-terminated quinoids: facile synthesis by Alkoxide-mediated rearrangement reaction and semiconducting properties. *Angew Chemie Int Ed* 59:221–225. <https://doi.org/10.1002/anie.201911530>
- [57] Asadi S, Mohammadi Ziarani G (2016) The molecular diversity scope of 1,3-indandione in organic synthesis. *Mol Divers* 20:111–152. <https://doi.org/10.1007/s11030-015-9589-z>
- [58] Singh K (2016) Applications of Indan-1,3-Dione in heterocyclic synthesis. *Curr Org Synth* 13:385–407
- [59] Pluskota R, Koba M (2018) Indandione and Its derivatives—chemical compounds with high biological potential. *Mini-Rev Med Chem* 18:1321–1330
- [60] Jayatunga MKP, Thompson S, McKee TC et al (2015) Inhibition of the HIF1 α -p300 interaction by quinone- and indandione-mediated ejection of structural Zn(II). *Eur J Med Chem* 94:509–516. <https://doi.org/10.1016/j.ejmech.2014.06.006>
- [61] Watt BE, Proudfoot AT, Bradberry SM, Vale JA (2005) Anticoagulant rodenticides. *Toxicol Rev* 24:259–269. <https://doi.org/10.2165/00139709-200524040-00005>
- [62] Amidi S, Kobarfard F, Bayandori Moghaddam A et al (2013) Electrochemical synthesis of novel 1,3-indandione derivatives and evaluation of their antiplatelet aggregation activities. *Iran J Pharm Res IJPR* 12:91–103
- [63] Leblois D, Piessard S, Le Baut G et al (1987) Pyrophtalones VII. Synthèse et activité anti-inflammatoire de (pyridinyl-4)-2 indanediones-1,3 substituées sur le noyau benzénique et/ou sur l'hétérocycle. *Eur J Med Chem* 22:229–238. [https://doi.org/10.1016/0223-5234\(87\)90054-7](https://doi.org/10.1016/0223-5234(87)90054-7)
- [64] Mishra CB, Manral A, Kumari S et al (2016) Design, synthesis and evaluation of novel indandione derivatives as multifunctional agents with cholinesterase inhibition, anti- β -amyloid aggregation, antioxidant and neuroprotection properties against Alzheimer's disease. *Bioorg Med Chem* 24:3829–3841. <https://doi.org/10.1016/j.bmc.2016.06.027>
- [65] Jeyachandran M, Ramesh P (2011) Synthesis, Antimicrobial, and Anticoagulant Activities of 2-(Arylsulfonyl)indane-1,3-diones. *Org Chem Int* 2011:360810. <https://doi.org/10.1155/2011/360810>
- [66] Wang Y, Liu H-X, Chen Y-C et al (2017) Two new metabolites from the endophytic fungus *Alternaria* sp. A744 derived from *Morinda officinalis*. *Molecules* 22:765. <https://doi.org/10.3390/molecules22050765>
- [67] Misra R, Pandey RC, Hilton BD et al (1987) Structure of fredericamycin A, an antitumor antibiotic of a novel skeletal type; spectroscopic and mass spectral characterization. *J Antibiot (Tokyo)* 40:786–802. <https://doi.org/10.7164/antibiotics.40.786>

- [68] Pandey RC, Toussaint MW, Stroshane RM et al (1981) Fredericamycin A, a new antitumor antibiotic. I. Production, isolation and physicochemical properties. *J Antibiot (Tokyo)* 34:1389–1401. <https://doi.org/10.7164/antibiotics.34.1389>
- [69] Warnick-Pickle DJ, Byrne KM, Pandey RC, White RJ (1981) Fredericamycin A, a new antitumor antibiotic II Biolproperties. *J Antibiot (Tokyo)* 34:1402–1407. <https://doi.org/10.7164/antibiotics.34.1402>
- [70] Mal D, Pahari P (2007) Recent advances in the Hauser annulation. *Chem Rev* 107:1892–1918. <https://doi.org/10.1021/cr068398q>
- [71] Janikowska K, Rachoń J, Makowiec S (2014) Acyl Meldrum's acid derivatives: application in organic synthesis. *Russ Chem Rev* 83:620–637. <https://doi.org/10.1070/rc2014v083n07abeh004441>
- [72] Jameel E, Umar T, Kumar J, Hoda N (2016) Coumarin: a privileged scaffold for the design and development of Antineurodegenerative agents. *Chem Biol Drug Des* 87:21–38. <https://doi.org/10.1111/cbdd.12629>
- [73] Grover J, Jachak SM (2015) Coumarins as privileged scaffold for anti-inflammatory drug development. *RSC Adv* 5:38892–38905. <https://doi.org/10.1039/C5RA05643H>
- [74] Stefanachi A, Leonetti F, Pisani L et al (2018) Coumarin: a natural, privileged and Versatile Scaffold for bioactive compounds. *Molecules* 23:250. <https://doi.org/10.3390/molecules23020250>

Publisher's Note Springer Nature remains neutral with regard to jurisdictional claims in published maps and institutional affiliations.